

# Modeling the gamma-ray emission in the Galactic Center with a fading cosmic-ray accelerator

Ruo-Yu Liu<sup>1</sup>, Xiang-Yu Wang<sup>2,3,1</sup>, Anton Prosekin<sup>1</sup>, Xiao-Chuan Chang<sup>2,3</sup>

## ABSTRACT

Recent HESS observations of the  $\sim 200$  pc scale diffuse gamma-ray emission from the central molecular zone (CMZ) suggest the presence of a PeV cosmic-ray accelerator (PeVatron) located in the inner 10 pc region of the Galactic Center. Interestingly, the gamma-ray spectrum of the point-like source (HESS J1745-290) in the Galactic Center shows a cutoff at  $\sim 10$  TeV, implying a cutoff around 100 TeV in the cosmic-ray proton spectrum. Here we propose that the gamma-ray emission from the inner and the outer regions may be explained self-consistently by run-away protons from a single, yet fading accelerator. In this model, gamma rays from the CMZ region are produced by protons injected in the past, while gamma rays from the inner region are produced by protons injected more recently. We suggest that the blast wave formed in a tidal disruption event (TDE) caused by the supermassive black hole (Sgr A\*) could serve as such a fading accelerator. With typical parameters of the TDE blast wave, gamma-ray spectra of both the CMZ region and HESS J1745-290 can be reproduced simultaneously. Meanwhile, we find that the cosmic-ray energy density profile in the CMZ region may also be reproduced in the fading accelerator model when appropriate combinations of the particle injection history and the diffusion coefficient of cosmic rays are adopted.

## 1. Introduction

Recently, the HESS collaboration reported the deep gamma-ray observations with arcminute angular resolution of the central molecular zone (CMZ) surrounding the center of our Galaxy (HESS Collaboration et al. 2016), extending out to  $r \sim 250$  pc and  $\sim 150$  pc at positive and negative Galactic longitudes respectively. The brightness distribution of very high energy (VHE) gamma rays shows a strong correlation with the locations of massive gas-rich complexes. This discovery, combined with the fact that in the leptonic scenario severe radiative losses would be expected for multi-TeV electrons in the Galactic Center, points to a hadronic origin of the diffuse VHE emission. The inferred radial profile of  $> 10$  TeV cosmic-ray (CR) energy density is consistent with  $1/r$  dependence in the entire CMZ region, and it was argued for a centrally located source in the inner  $\sim 10$  pc region with a quasi-constant injection operating over at least 1000 years,

---

<sup>1</sup>Max-Planck-Institut für Kernphysik, 69117 Heidelberg, Germany; ruoyu@mpi-hd.mpg.de

<sup>2</sup>School of Astronomy and Space Science, Nanjing University, Nanjing 210093, China; xywang@nju.edu.cn

<sup>3</sup>Key laboratory of Modern Astronomy and Astrophysics (Nanjing University), Ministry of Education, Nanjing 210093, China

given the diffusive propagation of cosmic rays (HESS Collaboration et al. 2016). The best-fit gamma-ray spectrum shows a single power-law form with a photon index of  $\sim 2.3$  extending to energies larger than tens of TeV without a break or a cutoff, which indicates the existence of a PeV proton accelerator, or the so-called "PeVatron".

Interestingly, the location of the PeVatron appears to coincide with the central point-like gamma-ray source HESS J1745-290, which shows a harder spectrum with a photon index of  $\sim 2.1$  and, however, a clear cutoff at  $\sim 10$  TeV (Aharonian et al. 2009). The GC has long been suggested as a cosmic-ray proton accelerator (e.g. Ptuskin & Khazan 1981; Said et al. 1981; Aharonian & Neronov 2005b; Liu et al. 2006; Fujita et al. 2016) and a hadronic origin was also suggested for the gamma-ray emission of HESS J1745-290 (Aharonian & Neronov 2005b; Chernyakova et al. 2011), while the leptonic origin may work well too (Aharonian & Neronov 2005a; Hinton & Aharonian 2007). There is no obvious connection between HESS J1745-290 and the gamma rays from the outer CMZ region. However, as protons accelerated at the center source will produce gamma rays via the proton–proton collision with the gas along the path to the outer CMZ region, they may potentially also explain the gamma-ray emission from HESS J1745-290 (Aharonian & Neronov 2005b; HESS Collaboration et al. 2016). In this scenario, some additional mechanisms must be introduced to reconcile the 10 TeV cut-off in the spectrum of HESS J1745-290 with the extension of the proton spectrum to PeV energies in the outer CMZ region. One possible solution is invoking the absorption due to a dense infrared photon field near the GC (HESS Collaboration et al. 2016). However, based on the current infrared data of the GC, the attenuation of the multi TeV photon flux originating from the GC is probably not strong enough to cause a cutoff (Moskalenko et al. 2006; Zhang et al. 2006; Aharonian et al. 2009; Celli et al. 2016), though an extremely clumpy distribution of the infrared photons might overcome this difficulty (Guo et al. 2016).

In this work, we propose a fading proton accelerator located at the inner 10 pc region as the origin of the gamma-ray emission from both HESS J1745-290 and the CMZ. In this model, the source was more powerful in the past and injected protons beyond PeV energies. These protons have propagated to the outer CMZ region, where, at the present time, they produce the gamma-ray emission with the spectrum extending to high energies. On the other hand, as the source power gradually fades and the maximum energy of the injected protons declines, the gamma-ray emission from the inner region, which arises from recently injected protons, develops a cutoff in the spectrum, which decreases towards the Galactic Center. We will show that this model explains simultaneously the gamma-ray spectra of the CMZ region and the inner point-like source.

As the particle injection rate of a fading accelerator decreases with time as well, it is apparently inconsistent with the suggestion by HESS Collaboration et al. (2016) that the CR energy density profile indicates a constant injection rate assuming a spatially independent diffusion coefficient. So we need to check whether the measured CR density profile can be reproduced in the fading accelerator model.

The rest part of this paper is organized as follows. We fit the gamma-ray spectral data of both the inner and outer region simultaneously in a specific scenario of fading accelerator, i.e., a tidal disruption event by the supermassive black hole in the Galactic Center drives a blast wave which accelerates cosmic rays

(§2). In §3, we study the energy density profile of cosmic rays in the general fading accelerator model, paying particular attention to the influence of the particle injection history and the diffusion coefficient. The discussion and conclusion are given in §4.

## 2. Modeling the gamma-ray spectra of the inner and outer regions

### 2.1. TDE blast wave as a fading particle accelerator

As the cosmic-ray acceleration process and injection history depends on the details of the accelerator, we now look for specific astrophysical sources that can act as such a fading accelerator and study whether the spectra of the inner and outer regions can be produced simultaneously in this scenario. HESS Collaboration et al. (2016) already pointed out that supernova remnants may not be responsible for the CRs, because the maximum proton energy will drop below PeV too quickly for a single SNR, while a high supernova rate in the central 10 pc seems unlikely. Limited by the position of the accelerator, HESS Collaboration et al. (2016) suggested the supermassive black hole at the GC (Sgr A\*) as the most plausible source for these CRs among several potential candidates.

We propose that a tidal disruption event (TDE) by the supermassive black hole at the GC could be such a fading accelerator. When a star gets too close to the supermassive black hole, it will be disrupted by the tidal force of the black hole (e.g. Hills 1975; Carter & Luminet 1982; Rees 1988), leading to a transient accretion disk and sometimes also a relativistic outflow. There are growing number of candidate TDEs occurred in other galaxies that have been discovered in X-ray, ultraviolet, and optical surveys (see Komossa 2015 for a review). Three TDE candidates have been also detected in non-thermal X-ray and radio emission, i.e., Swift J1644+57 (Bloom et al. 2011), J2058+05 (Cenko et al. 2012), and J1112-8238 (Brown et al. 2015). The non-thermal X-ray and radio emissions are thought to be produced by relativistic jets, in which shocks occur and accelerate non-thermal electrons. The isotropic radiation energies in X-rays in all three jetted TDEs are about  $3 \times 10^{53}$  erg, so the isotropic kinetic energy of the jets are of the order of  $10^{54}$  erg. Assuming an opening angle of  $\theta_j \sim 0.1$ , the real jet energy is about  $10^{52}$  erg. The event rate of TDEs caused by supermassive black holes of mass  $10^6 - 10^7 M_\odot$  is about  $10^{-5} - 10^{-4} \text{ yr}^{-1}$  per galaxy (Wang & Merritt 2004; Stone & Metzger 2016). Interestingly, it has been suggested that TDEs in the GC can power the diffuse gamma-ray emission in the GC via hadronic interactions (Cheng et al. 2007; Chen et al. 2016). We here suggest that the TDE blast wave is a fading accelerator and it can explain both gamma-ray emission spectrum and the CR density profile in the GC. In the calculation below, we use eV as the unit of particle energy and c.g.s units for other quantities. We denote by  $Q_x$  the value of the quantity  $Q$  in units of  $10^x$  unless specified.

The TDE jet expands sideways when its Lorentz factor drops to  $\Gamma \lesssim 1/\theta_j$ , and the blast wave approaches spherical symmetry soon after it enters the sub-relativistic phase (Livio & Waxman 2000). Later on, being decelerated further by the ambient medium, the blast wave enters the non-relativistic phase (the Sedov phase) at

$$t_s = [3E/(4\pi n m_p c^5)]^{1/3} = 0.06 E_{52}^{1/3} n_4^{-1/3} \text{ yr} \quad (1)$$

where  $n$  is the number density of gas in the GC region. This time is shorter than one year for typical parameters. In the Sedov phase, the speed of the blast wave (in units of the light speed) is

$$\beta = \left( \frac{12E}{125\pi n m_p c^5 t^3} \right)^{1/5} = 4.7 \times 10^{-4} E_{52}^{1/5} n_4^{-1/5} \left( \frac{t}{10^4 \text{yr}} \right)^{-3/5}. \quad (2)$$

The radius of the blast wave is then

$$R = \frac{5}{2} \beta c t = 3.6 E_{52}^{1/5} n_4^{-1/5} \left( \frac{t}{10^4 \text{yr}} \right)^{2/5} \text{ pc}. \quad (3)$$

To estimate the maximum CR proton energy accelerated by the blast wave, we adopt the formula given by Bell et al. (2013, also see Bell 2015), which considers the amplification of magnetic field by the non-resonant hybrid instability, i.e.,

$$E_{p,\text{max}} = 55 \eta_{0.1} E_{52}^{3/5} n_4^{-1/10} \left( \frac{t}{10^4 \text{yr}} \right)^{-4/5} \text{ TeV}. \quad (4)$$

Note that here we have already substituted the evolution of shock velocity and shock radius into the original equation.  $\eta_{0.1}$  is the acceleration efficiency normalized to 0.1<sup>1</sup>. The time-dependent behavior of the maximum energy  $E_{\text{max}}$  is important for the spectral fitting. If  $E_{\text{max}}$  decreases faster, the two cutoff energies in the respective spectra of the inner region and the CMZ region would have larger difference. So that the spectrum of the CMZ region can extend up to higher energies while the spectrum of the inner region keeps the same cutoff energy.

The total luminosity of cosmic rays in the Sedov phase can be estimated as (Gabici 2011)

$$L_p(t > 1 \text{ GeV}) = f_{\text{CR}} \frac{n m_p u_{\text{sh}}^3}{2} 4\pi R^2 = 3.6 \times 10^{40} f_{\text{CR}} E_{52} \left( \frac{t}{10^4 \text{yr}} \right)^{-1} \text{ erg/s}, \quad (5)$$

where  $u_{\text{sh}} = \beta c$  is the velocity of the blast wave and  $f_{\text{CR}}$  is the fraction of the kinetic energy of the blast wave that goes into injected CRs.  $f_{\text{CR}}$  is at the level of  $\sim 1\% - 10\%$  for the blast waves of supernova remnants, according to the gamma-ray analysis on our Galaxy (Strong et al. 2010) and nearby starburst galaxies (Paglione & Abrahams 2012; Peng et al. 2016). For simplicity, we use a time-independent  $f_{\text{CR}}$ .

We note that the dynamic evolution of the blast wave driven by TDE should be identical to that of the supernova remnant except for the one-order-of-magnitude larger kinetic energy, since both follow the Sedov solution. This larger kinetic energy leads to a  $E_{p,\text{max}}$  larger by a factor of several compared with the supernova remnant case at the same time, which is crucial to the fitting of the gamma-ray spectrum of the CMZ region at highest energy bins. As can be seen in the next subsection (Fig. 1), we may not get an

---

<sup>1</sup>The value of  $\eta$  is estimated to be 0.03 in Bell et al. (2013), assuming that only CRs of the highest-energy decade escape and drive the instability. However, gamma-ray observations of many CR-illuminated molecular clouds indicate a broad-spectrum escape of CRs from supernova remnant (e.g., Aharonian et al. 2008; Abdo et al. 2010; Uchiyama et al. 2012; Ackermann et al. 2013, see also Malkov et al. 2013), rather than a high-energy-biased escape. Since the growth rate of the instability is proportional to the escaping CR current, consideration of a broad-spectrum escape of CRs could increase this the efficiency by an order of magnitude.

acceptable fitting to the spectrum of the CMZ region if  $E_{p,\max}$  is several times smaller. However, in the case of a hypernova explosion or some other events which release a comparable kinetic energy ( $\gtrsim 10^{52}$  erg) to a TDE, the result would be quite similar.

## 2.2. The gamma-ray spectra of the inner and outer regions

We now look further into the gamma-ray production during the propagation of CRs, aiming to simultaneously reproduce the gamma-ray spectra of both the central point-like source and the outer CMZ region measured by HESS.

Assuming that the cosmic-ray injection spectrum follows  $J_p(E_p, t) = C(t)E_p^{-s} \exp(-E_p/E_{p,\max})$ , we can find the normalization factor  $C(t)$  as  $C(t) = L_p(t) / \int_{1\text{ GeV}}^{\infty} E_p^{1-s} \exp(-E_p/E_{p,\max}) dE_p$ . Since the observed gamma-ray spectral index of HESS J1745-290 is about 2.1, the value of  $s$  should be around 2.2 as the cross section of  $pp$ -collision increase roughly with energy as  $E^{0.1}$  beyond the threshold energy. While the cosmic-ray spectral shape follows the injected one in the inner region where particles still propagate rectilinearly, the spectral shape in the outer region is affected by diffusion. Given that the energy dependence of the diffusion coefficient follows the form

$$D(E_p) = 10^{30} \left( \frac{D(10\text{ TeV})}{10^{30}\text{ cm}^2/\text{s}} \right) \left( \frac{E_p}{10\text{ TeV}} \right)^{\delta} \text{ cm}^2/\text{s} \quad (6)$$

with  $\delta$  usually being in the range of 0–1, the CR spectrum index becomes  $s+\delta$  in the diffusion region. Since the gamma-ray spectral index of the CMZ region is  $\sim 2.3$ , we adopt  $\delta = 0.2$ .

To find the spatial distribution of CRs, we consider a temporally and spatially independent diffusion coefficient  $D(E_p)$ , and assume that injection and diffusion have spherical symmetry. Then the probability of finding one particle at distance  $r$  away from the source at a time  $t$  after its injection is given by (Aloisio et al. 2009; Dunkel et al. 2007)

$$P(E_p, t, r) = \frac{\theta(ct - r)}{(ct)^3 Z\left(\frac{c^2 t}{2D(E_p)}\right) \left[1 - \left(\frac{r}{ct}\right)^2\right]^2} \exp\left[-\frac{\frac{c^2 t}{2D(E_p)}}{\sqrt{1 - \left(\frac{r}{ct}\right)^2}}\right], \quad (7)$$

where  $Z(y) = 4\pi K_1(y)/y$  with  $K_1$  being the first-order modified Bessel function, and  $\theta$  is the Heaviside function. This function works for both the rectilinear propagation of particles at  $r \ll D(E_p)/c$  and the diffusive propagation at  $r \gg D(E_p)/c$ , as well as for the transition regime of the two propagation modes. We note that the inclusion of both diffusion and rectilinear regimes of propagation is a necessary for fitting, as the spectra of the gamma-ray emissions from CMZ and HESS J1745-290 have different spectral indices. Indeed, the change of spectral features from one region to another, assuming a single CR source, indicates the changes either in the injection spectrum or in the propagation regime of CRs. Since we assume that the index of the injection spectrum is constant, we should consider the change in the propagation regime. We neglect the energy losses of CRs during their propagation via the  $pp$ -collision, since the energy loss time,  $t_{pp} \simeq 5 \times 10^5 \left(\frac{n}{100\text{ cm}^{-3}}\right)^{-1} \text{ yr}$ , is much longer than the propagation time to a distance of 200 pc,  $t_{\text{diff}} \simeq$

$10^4 \left(\frac{r}{200\text{pc}}\right)^2 \left(\frac{D}{10^{30}\text{cm}^2/\text{s}}\right)^{-1}$  yr, unless the diffusion coefficient is  $\ll 10^{29}\text{cm}^2/\text{s}$ . Due to the similar reason, the advection of cosmic rays with a possible wind/outflow of a bulk velocity  $v_w$  launched from the GC may be negligible given the advection timescale  $t_{\text{adv}} \simeq 2 \times 10^5 \left(\frac{r}{200\text{pc}}\right) \left(\frac{v_w}{1000\text{km/s}}\right)$  yr, which is also much longer than the diffusion timescale.

The radial distribution of CR energy density at  $t_0$  after the occurrence of a TDE can then be obtained by

$$n_p(E_p, r, t_0) = \int_0^{t_0} P(E_p, t_0 - t, r) J_p(E_p, t) dt, \quad (8)$$

Once the spatial distribution of the protons is obtained, we can calculate the gamma-ray production rate in the ambient hydrogen gas. Here we adopt the parametrized analytical formula for gamma-ray emission of  $pp$ -collision given by (Kelner et al. 2006)

$$\dot{q}_\gamma(E_\gamma, r) \equiv \frac{d\dot{N}_\gamma}{dE_\gamma} = cn(r) \int_{E_\gamma}^{\infty} \sigma_{pp}(E_p) n_p(E_p, r) F_\gamma\left(\frac{E_\gamma}{E_p}, E_p\right) \frac{dE_p}{E_p}. \quad (9)$$

where  $n_p(r)$  is the density of the hydrogen gas at a radial distance  $r$  to the GC,  $\sigma_{pp}$  is the cross section for the  $pp$ -collision and  $F_\gamma$  dictates the distribution of secondary gamma rays. For simplicity, we assume two different uniform densities for inner 15 pc region and the outer region respectively, while their values are chosen to fit the measured spectral data. Then, by assuming the disk radius to be 250 pc and the disk height to be 70 pc, we integrate over the gamma-ray flux from the very center up to a projection distance of 15 pc, and from 15 pc up to 70 pc to obtain the theoretical gamma-ray flux of HESS J1745-290 and CMZ regions respectively (see the Appendix for details).

In Fig. 1, fixing the injection time  $t_0 = 10^4$  yr (i.e., the TDE occurred at  $10^4$  years ago), we fit the gamma-ray spectra of both the CMZ region and HESS J1745-290 with the fading TDE blast wave model. The spectrum of the CMZ region starts to drop at  $\gtrsim 10$  TeV because the maximum proton energy in the outer region already starts to fall below PeV, but the fitting is still consistent with the HESS data at  $1\sigma$  confidence level, with a reduced chi-square of 31.4/17<sup>2</sup>. We do not consider the flux attenuation via  $\gamma\gamma$  absorption by interstellar background photons as it is not important in the considered energy range (e.g., Porter & Strong 2005; Moskalenko et al. 2006; Celli et al. 2016). The fitting to the spectrum of HESS J1745-290 yields a reduced chi-square of 27.2/19, also at  $1\sigma$  confidence level. Technically, we could adopt a larger acceleration efficiency  $\eta$  and/or a larger explosion energy  $E$  (see Eq. 4) to increase the maximum energy and thus improve the fitting to the spectrum of the CMZ region, however, at the expense of the gamma-ray flux from the inner

---

<sup>2</sup> The best fitting would result in a minimum reduced chi-square of 1 at least. Given a degree of freedom of 17 (22 data points – 5 free parameters), the corresponding reduced chi-square for  $1\sigma$  boundary should be  $> 2.13$ . So our fitting must be within the  $1\sigma$  confidence level although we do not obtain the best fitting here. For the same reason we state that other fittings are also within  $1\sigma$  confidence level in the text below (The 5 free parameters used in the profile fitting are the diffusion coefficient for 10 TeV proton, the normalization, power-law index and the cutoff energy of the proton injection spectrum, and the gas density. Other parameters are either determined by the model in advance or derived according to these parameters)

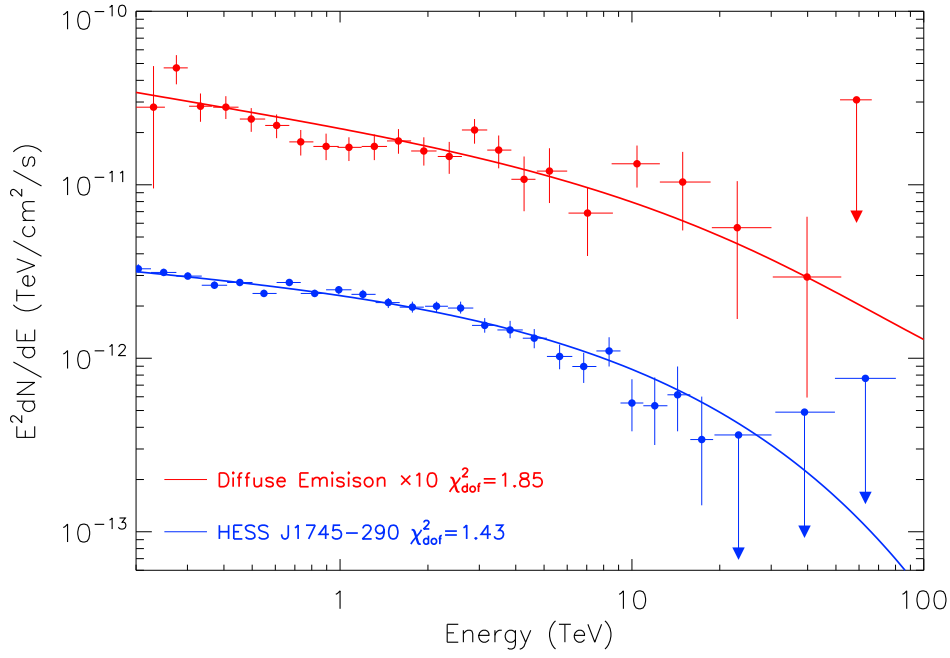


Fig. 1.— Fitting the gamma-ray spectra of the CMZ region (red) and HESS J1745-290 (blue). The adopted parameters in the calculation are given in Table. 1. All the data are taken from HESS Collaboration et al. (2016).

15 pc significantly exceeding the  $2\sigma$  upper limit in the spectrum of HESS J1745-290 at 20–30 TeV. In this case, considering a clumpy distribution of infrared photon field in the inner region would enhance the absorption and lead to a decrease or even a cutoff in the spectrum of the inner region (cf Guo et al. 2016). Besides, the fitting can be ameliorated by a further fine-tuning of the adopted parameters. For simplicity, we adopt some typical values for the parameters, which are shown in Table 1. The gas density used for the inner 15 pc is several tens times higher than that of the outer region. This might reflect the density difference between the core region of the central molecular zone and its average value. The radius of the blast wave at  $t_0 = 10^4$  yr is still within 10 pc, which is consistent with the HESS measurement. The adopted parameters result in a total proton luminosity ( $> 1$  GeV) of about  $6 \times 10^{38}$  erg/s at the present time. Although this value is about three orders of magnitude higher than the current bolometric luminosity of Sgr A\* (Genzel et al. 2010), it reflects the past activity of the supermassive black hole.

Adopted Parameters & Resulting Parameters			
$E$	$1.1 \times 10^{52}$ erg	$L_p^t (> 1 \text{ GeV})$	$6.3 \times 10^{38}$ erg/s
$s$	2.15	$E_{p,\text{max}}^t$	150 TeV
$D(10 \text{ TeV})$	$3.3 \times 10^{30} \text{ cm}^2/\text{s}$	$\delta$	0.2
$\eta$	0.25	$\beta^t$	$4.7 \times 10^{-4}$
$f_{\text{CR}}$	1.8%	$R^t$	4.1 pc
$n(\text{CMZ region})$	$150 \text{ cm}^{-3}$	$n(\text{central region})$	$5000 \text{ cm}^{-3}$

Table 1: Parameters used in Fig. 1. Parameter with the superscript ‘ $t$ ’ means the quantity is time-dependent and the shown value is the present-time value.

### 3. Cosmic ray energy density profile in the fading accelerator scenario

Using the spatial distribution of the gamma-ray intensity and the amount of target gas in the CMZ, HESS Collaboration et al. (2016) has obtained the projected profile of the  $E \geq 10$  TeV CR energy density up to  $r \simeq 200$  pc. Assuming a spatially independent diffusion coefficient, HESS Collaboration et al. (2016) found that the data is consistent with a constant injection rate of CRs, which is in contrast to a decreasing injection rate in our model. Below we study the expected cosmic ray energy density profile from a fading accelerator and compare it with the HESS measurements.

First, we use Eq. (8) and the parameters obtained from the spectral fitting (see Table.1) to calculate the CR energy density profile in the TDE blast wave scenario. Eq. (8) already gives the radial distribution of CR number density. We need to integrate it over energy to get the radial distribution of CR energy density and then average over the line of sight to get the projected profile of CR energy density (see Appendix for details). The fit to the data is shown in Fig. 2, which gives a reduced chi-square of 12.2/6. The theoretical curve is within the  $1\sigma$  deviation of the HESS data.

We note that the CR energy density profile is sensitive to CR injection history which depends on the specific accelerator models, while the TDE blast wave is just one example of the accelerators. Meanwhile,



the CR diffusion coefficient in the CMZ region, which is not well-understood, also affects the CR energy density profile, as it determines whether the propagation mode of CRs at certain distance is rectilinear or diffusive. So we perform a general study on how the CR injection history and diffusion coefficient affect the CR energy density profile.

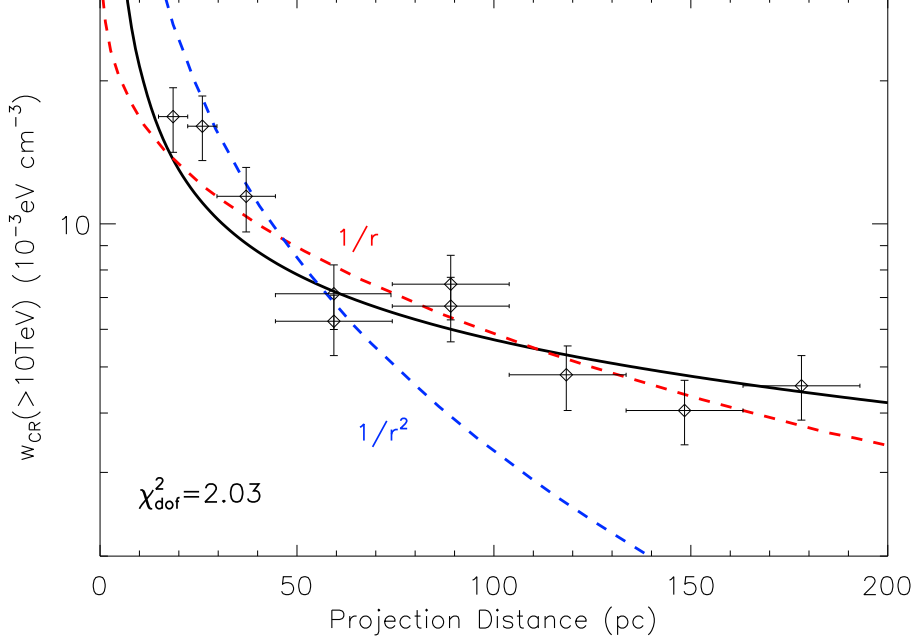


Fig. 2.— Fitting to the measured CR energy density under the TDE blast wave model with the same parameters in Table.1. The black curve is calculated by averaging over the CR energy density in the line of sight for each given projection distance to the GC, yielding a reduced chi-square of 2.03. Open diamonds are measured data, the red and blue dashed lines represent the performance of the projection of a  $1/r$  and a  $1/r^2$  profile respectively, as shown in the Figure 2 in HESS Collaboration et al. (2016).

We parametrize the particle luminosity at  $E_p$  as  $L(t, E_p) = L_*(t/t_*)^{-\alpha}$  with  $t_*$  being the time when the luminosity starts to follow the assumed form and  $\alpha$ . Then, we can write the energy density distribution of cosmic rays at  $t_0$  as

$$w(E_p, r) = \int_{t_*}^{t_0} P(E_p, t_0 - t, r) L(t, E_p) dt. \quad (10)$$

We fix  $t_* = 0.1$  yr in our calculation, though we note that the obtained density at  $r$  is not sensitive to  $t_*$  as long as  $t_0 - t_* \gg r^2/D(E_p)$ . Following our previous assumption of a gas disk of radius 250 pc, we average over the CR density along the line of sight to get the projected CR energy density profile and then compare it with the measurement of HESS. The obtained CR energy density profile is mainly determined by the injection time  $t_0$ , the power-law slope of the injection rate history  $\alpha$  and the diffusion coefficient  $D(E_p)$ . In the following

calculation, we will fix  $t_0$  at certain values and change the other two quantities. To save the calculation time, we consider a mono-energetic injection of CRs at  $E_p = 10$  TeV and calculate the 10 TeV CR energy density profile. Although what HESS measures is the integrated CR energy density above 10 TeV, this simplification does not introduce much error since most of the CR energies above 10 TeV concentrate on 10 TeV for a soft CR spectral index of 2.4 at the CMZ region.

The results with different injection time of  $t_0 = 10^3$  yr,  $10^4$  yr,  $10^5$  yr and  $10^6$  yr are shown in different panels in Fig. 3. The reduced chi-square test is used to evaluate the goodness of fit. Different colors represent the corresponding values (see the color bar) of the reduced chi-square ( $\chi^2_{\text{dof}}$ ) for each combination of  $\alpha$  and  $D$ .  $1\sigma$ ,  $2\sigma$ ,  $3\sigma$  confidence regions are marked in the figure, as well as the contours for  $\chi^2 = 1.2, 10$  for comparison. Since  $L_*$  only relates to the amplitude of the energy density profile, we do not concern ourselves with it and its value is chosen to get the minimum chi-square for the given values of  $\alpha$  and  $D$ . The inset figure in each panel shows the fit to the measured CR energy density profile with the best-fit parameters for a given  $t_0$ . We find that a decreasing injection rate with  $\alpha \sim 0.5 - 1.0$  and a large diffusion coefficient  $\gtrsim 10^{30.5} \text{ cm}^2/\text{s}$  for 10 TeV protons can give good fitting to the measured data. We can also see the deviation from the data in the TDE blast wave model, in which  $t_0 = 10^4$  yr,  $\alpha = 0.8$  and  $D(10 \text{ TeV}) = 3.3 \times 10^{30} \text{ cm}^2/\text{s}$ , is  $< 1\sigma$ , being consistent with the result in Fig.2.

The decreasing injection rate of a fading source leads to the flattening of the spatial distribution of CR density, compared to the measured  $\sim 1/r$  dependence which arises from a constant injection with a spatially independent diffusion coefficient. However, a large diffusion coefficient results in a transition to the  $\sim 1/r^2$  dependence for the rectilinear regime at small distances, which alleviates this problem, leading to a reasonable fit to the data. Actually, for a small  $t_0$  and a small  $D$ , constant injection does not give a very good fitting to the data. This is because some particles have not diffused to large  $r$  for a finite injection time  $t_0$  and, hence, the profile can not keep the  $1/r$  form<sup>3</sup>. We note that the favored diffusion coefficient in the fit is about one order of magnitude larger than that in the Galactic disk at the same energy, which is  $\sim 10^{28} \text{ cm}^2/\text{s} (E/1 \text{ GeV})^{1/3}$  (e.g. Strong et al. 2010). However, the diffusion coefficient in the CMZ region is unclear currently. Indeed, due to the different environment at the Galactic Center and the Galactic disk, the diffusion coefficients in these two regions may be different. We will further discuss the diffusion coefficient in the next section.

#### 4. Discussions and Conclusions

In this work, we proposed a fading accelerator located in the inner 10 pc of the GC as the source for the gamma-ray emission of both the point-like source HESS J1745-290 and the CMZ region. Given the decreasing maximum acceleration energy in the injected proton spectrum, gamma rays of the inner region presents a cutoff around 10 TeV as they are produced via  $pp$ -collision by more recently injected protons that

---

<sup>3</sup>Mathematically, in the purely diffusion regime, a constant injection rate  $L$  leads to a distribution of energy density as  $\frac{L}{4\pi Dr} \text{erfc}\left(\frac{r}{\sqrt{4Dt}}\right)$  (Atoyan et al. 1995). The profile starts to drop when  $r$  approaches  $\sqrt{4Dt}$ .

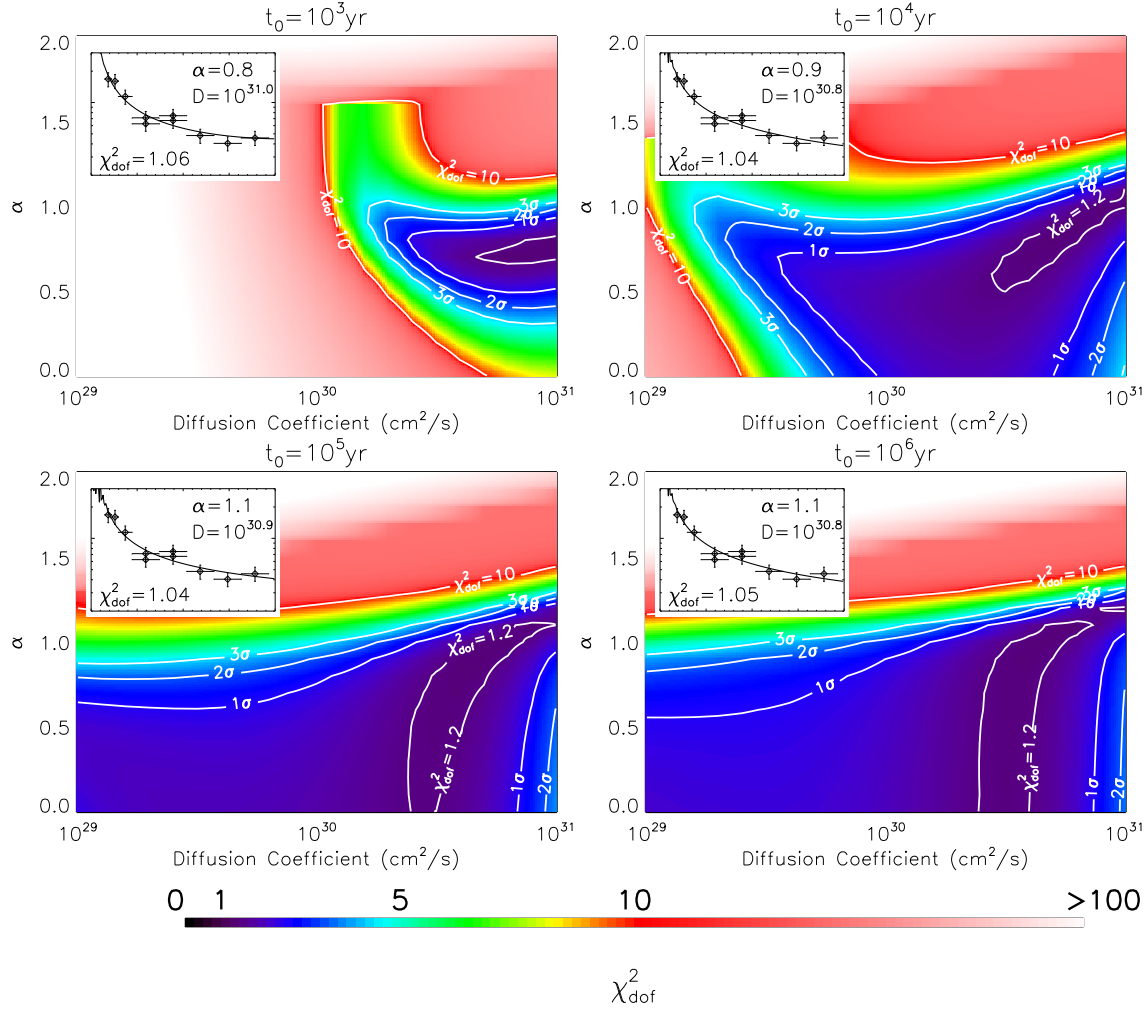


Fig. 3.— The reduced chi-square for different combinations of injection history  $\alpha$  and diffusion coefficient  $D$  for 10 TeV protons given different injection time. Different colors corresponds to different values of the reduced chi-square, as shown in the color bar in the bottom. Note that the color changes linearly in the range of  $\chi^2_{\text{dof}} = 0-10$  and logarithmically in the range of  $10-100$ . The  $1\sigma$ ,  $2\sigma$ ,  $3\sigma$  confidence region as well as the contours for  $\chi^2_{\text{dof}} = 1.2$ ,  $10$  are marked in the figure. The inset figures show the best fits to the measured CR energy density in the considered range of  $\alpha$  and  $D$ .

have a lower maximum energy, while the gamma rays of the outer CMZ region arise from earlier injected protons that have a larger maximum energy and hence produce a spectrum extending to energies beyond tens of TeV. The fading accelerator could be due to some past activity of the supermassive black hole, such as a blast wave driven by a TDE due to the supermassive black hole in the GC. Following the Sedov solution of the blast wave, we obtained the evolution of the particle injection rates and maximum acceleration energy in such a scenario. A simultaneous fit to the spectra of both HESS J1745-290 and the CMZ region is obtained within  $1\sigma$  deviation from the HESS data. We find that the measured CR energy density profile can also be reproduced with the same parameters. Furthermore, we performed a general study of the effects of the CR injection history and the diffusion coefficient on the resultant energy density profile and found that the fading accelerator can reproduce the measured data for different injection times.

It may be worth noting the possibility that gamma rays in the inner region may have a different origin from that in the outer CMZ region. In this case, the fading accelerator model can still account for the gamma-ray emission in the CMZ region and the fit to the data could be improved as there is no constraints from the inner source anymore. We may adopt a larger kinetic energy and/or a higher acceleration efficiency to get a higher  $E_{\text{max}}$ , so that the calculated spectrum in the CMZ region can extend up to tens of TeV without softening. In the meanwhile, we need to adopt a lower hydrogen gas density for the inner region in order not to overshoot the observed gamma-ray flux of HESS J1745-290.

As we already mentioned in the last section, to obtain a good fit to the CR energy density profile, the favored diffusion coefficient in the CMZ region is about one order of magnitude larger than that in the Galactic disk. Such a large diffusion coefficient would lead to a purely rectilinear propagation regime of CRs inside the inner  $\ll D/c \sim 30$  pc, which also implies that CRs are still not fully isotropized even at tens of pc (Prosekin et al. 2015). The gamma-ray fluxes from such regions are enhanced (reduced) if the most CRs are moving towards (away from) our line of sight. This is because the emitted gamma-rays will concentrate on the moving direction of their ultra-relativistic parent protons (i.e., the beaming effect). As a result, we may underestimate the gamma-ray flux from the HESS J1745-290 while overestimate the gamma-ray flux from the CMZ region, as we have assumed CRs are isotropized in our calculation. However, we note that the theoretical flux of HESS J1745-290 is barely affected by this effect. This is because, given a much higher gas density in the inner 15 pc region than the outer region, the flux of HESS J1745-290 should be dominated by the emission from the inner 15 pc region, which has spherical symmetry in our model. So the enhanced flux is exactly balanced by the shrunk observable region. The extent of the overestimation on the flux of the CMZ region depends on how far the real distribution of CRs deviate from the isotropic one. Since the pitch angle distribution of CRs becomes broader as they propagate, we may expect a typical angular size of a bundle of CRs after propagation a distance of  $r$  as (Prosekin et al. 2015)

$$\theta = \sqrt{\frac{2r}{3D/c}}. \quad (11)$$

Substituting the obtained parameters into the above equation, we find that the angular size of 100 TeV protons is about  $30^\circ$  at 20 pc and  $50^\circ$  at 70 pc, implying a considerable fraction of CRs that initially propagate away from us are already deflected to our direction. Besides, CRs are already isotropized at larger radius. So

we may expect that the overestimation of the flux from the CMZ region is not severe and can be modulated by tuning the gas density in the CMZ region.

To simplify the calculation, several assumptions have been made in our calculations, such as a uniform gas density, a spatially independent and isotropic diffusion coefficient, a temporally independent particle acceleration and injection efficiency, and etc. We note that the large diffusion coefficient may be avoided if more complicated factors are taken into account. For example, if the diffusion coefficient is spatially dependent, such as increasing outwardly, a smaller diffusion coefficient might also work. This is due to that a faster diffusion (i.e., larger  $D$ ) leads to a smaller density, so an outwardly increasing diffusion coefficient could yield a steeper profile of CR energy density compared with that in the case of a spatially independent diffusion coefficient, and hence fit the data with a smaller diffusion coefficient at the GC. Besides, if we consider the capability of the confinement of CRs by the blast wave decreases with time (i.e.,  $f_{\text{CR}}$  increases with time), the injection rate would decrease less rapidly with time, and then a smaller diffusion coefficient could also work well in fitting the CR density profile. More realistic modeling using complicated numerical calculations/simulations on the relevant processes would be useful for a more careful study. We leave this study to a future publication.

In the present model, cosmic rays are injected by a fading accelerator, probably arising from some types of explosion events, such as a TDE. Provided that the event rate of the explosion is  $10^{-5} - 10^{-4} \text{ yr}^{-1}$ , such a fading accelerator would occur repeatedly on the timescale of  $> 10^5 \text{ yr}$ . In this sense, the particle injection rate appears to be quasi-constant on such long timescales. Indeed, there may be no strict constant injection in nature. Every source may be variable at different time scales. We note that the measured gamma-ray emission in the CMZ region probes the CR injection on a time scale of  $10^3 - 10^4 \text{ yr}$  or longer, while the gamma-ray from the inner 10 pc mainly reflects the CR injection in recent 10–100 yr. Thus, one alternative scenario is that the source (quasi-)constantly injected CRs (i.e.,  $\alpha = 0$ ) with a spectrum extending up to  $> \text{PeV}$  during the past ten thousand years or longer while the source is variable on a short timescale of 10–100 yr. Coincidentally, it is just in a less active period during the recent ten years, resulting in a low particle acceleration efficiency and, subsequently, the cutoff in the measured spectrum of the inner region. A further study on the CR acceleration and injection is required to reveal more details in this scenario, which, however, is beyond the scope of this work.

We thank Felix Aharonian for the valuable comments and suggestions, and thank Tony Bell for the helpful discussions. This work is supported by the National Basic Research Program (973 Program) of China under Grant No. 2014CB845800, the National Natural Science Foundation of China under Grants No. 11273016 and No. 11625312.

### A. Average/Integration over line of sight

The geometry of the central molecular zone including the inner region in our model is shown as Fig. 4. We assume the outermost radius of the disk is  $R_d = 250 \text{ pc}$  and the thickness of the disk is 140 pc (or with a

height  $H_{\max} = 70 \text{ pc}$ ). The line-of-sight average CR density in the disk plane is given by

$$\bar{w}_{CR}(> 10 \text{ TeV}, R_{\text{proj}}) = \frac{1}{l_{\max}} \int_0^{l_{\max}} w(> 10 \text{ TeV}, r) dl \quad (\text{A1})$$

where  $l_{\max} = \sqrt{R_d^2 - R_{\text{proj}}^2}$  and  $r = \sqrt{l^2 + R_{\text{proj}}^2}$ .

The line-of-sight integrated gamma-ray flux from the center ( $r = 0$ ) to a circle with a projected radius of  $R_{\text{proj}}$  is

$$F_{\gamma}(E; 0, R_{\text{proj}}) = \frac{8}{4\pi d^2} \int_0^{R_{\text{proj}}} dh \int_0^{r_{\text{proj},\max}(h)} dr_{\text{proj}} \int_0^{l_{\max}} \dot{q}_{\gamma}(r, E) dl \quad (\text{A2})$$

where  $q_{\gamma}(r, E)$  is the gamma-ray emissivity in unit volume at energy  $E$  at a radial distance  $r = \sqrt{l^2 + r_{\text{proj}}^2} + h^2$  to the center.  $d = 8.5 \text{ kpc}$  is the distance between the GC and the Earth. The upper limit in the integration  $r_{\text{proj},\max}(h) = \sqrt{R_{\text{proj}}^2 - h^2}$  and  $l_{\max} = \sqrt{r_{\text{proj},\max}^2 - r_{\text{proj}}^2}$ . The factor 8 arises from the fact that the above integration actually counts only 1/8 of the total emission of the considered region given the symmetry in the distribution gamma-ray emissivity density. To obtain the line-of-sight integrated gamma-ray flux within a ring from a projected radius of  $R_{\text{proj},\min}$  to  $R_{\text{proj},\max}$ , we need to perform the calculation  $F_{\gamma}(E; R_{\text{proj},\min}, R_{\text{proj},\max}) = F_{\gamma}(E; 0, R_{\text{proj},\max}) - F_{\gamma}(E; 0, R_{\text{proj},\min})$ .

## REFERENCES

- Abdo, A. A., Ackermann, M., Ajello, M., et al. 2010, *ApJ*, 718, 348
- Ackermann, M., Ajello, M., Allafort, A., et al. 2013, *Science*, 339, 807
- Aharonian, F., Akhperjanian, A. G., Anton, G., et al. 2009, *A&A*, 503, 817
- Aharonian, F., Akhperjanian, A. G., Bazer-Bachi, A. R., et al. 2008, *A&A*, 481, 401
- Aharonian, F., & Neronov, A. 2005a, *ApJ*, 619, 306
- . 2005b, *Ap&SS*, 300, 255
- Aloisio, R., Berezhinsky, V., & Gazizov, A. 2009, *ApJ*, 693, 1275
- Atoyan, A. M., Aharonian, F. A., & Völk, H. J. 1995, *Phys. Rev. D*, 52, 3265
- Bell, A. R. 2015, *MNRAS*, 447, 2224
- Bell, A. R., Schure, K. M., Reville, B., & Giacinti, G. 2013, *MNRAS*, 431, 415
- Bloom, J. S., Giannios, D., Metzger, B. D., et al. 2011, *Science*, 333, 203
- Brown, G. C., Levan, A. J., Stanway, E. R., et al. 2015, *MNRAS*, 452, 4297
- Carter, B., & Luminet, J. P. 1982, *Nature*, 296, 211

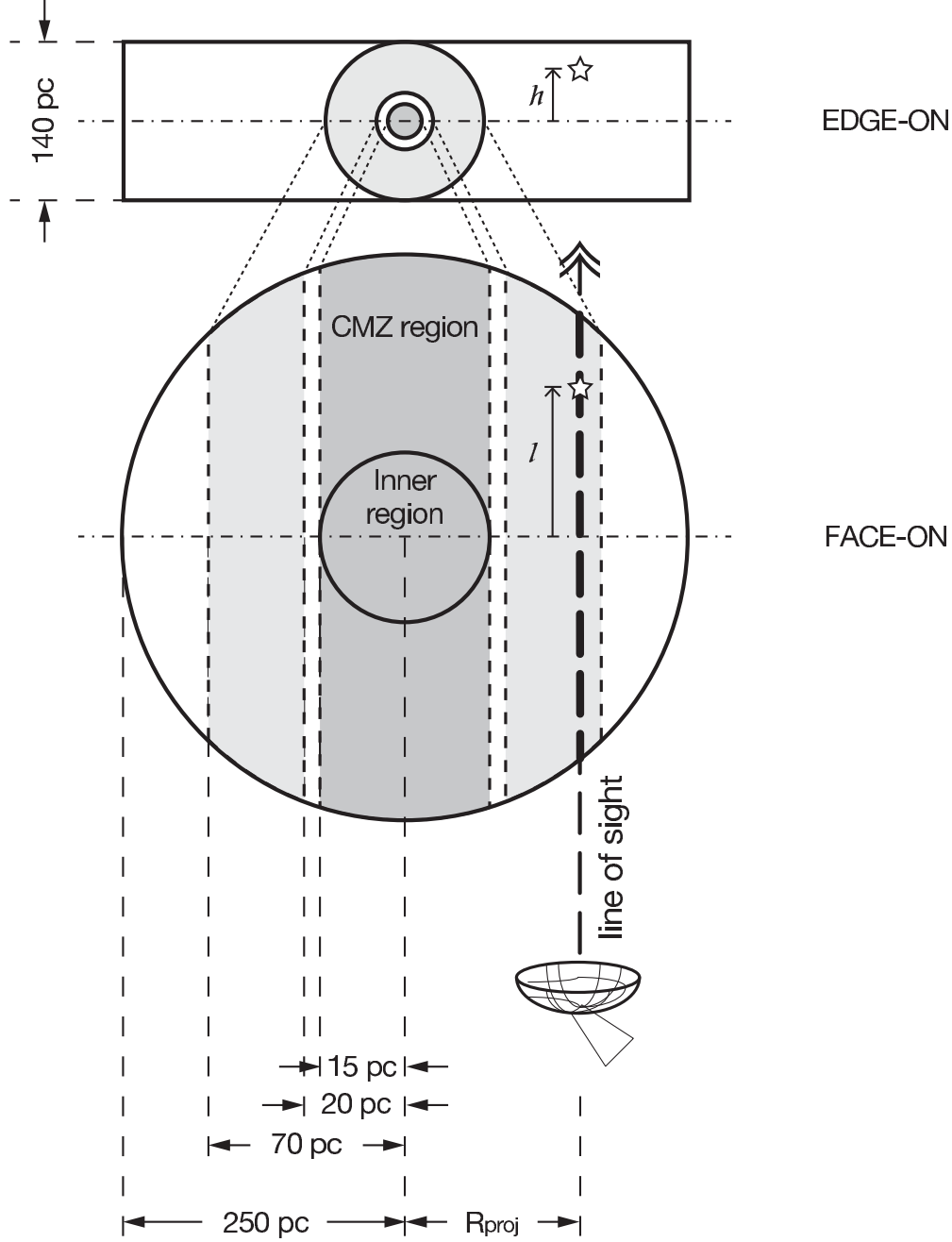


Fig. 4.— A sketch for the geometry of the gas disk at the GC used in our calculation. The darker and lighter hatched regions are the spectrum extracting region of HESS J1745-290 and the CMZ region respectively.

- Celli, S., Palladino, A., & Vissani, F. 2016, ArXiv e-prints, arXiv:1604.08791
- Cenko, S. B., Krimm, H. A., Horesh, A., et al. 2012, *ApJ*, 753, 77
- Chen, X., Gómez-Vargas, G. A., & Guillochon, J. 2016, *MNRAS*, 458, 3314
- Cheng, K. S., Chernyshov, D. O., & Dogiel, V. A. 2007, *A&A*, 473, 351
- Chernyakova, M., Malyshev, D., Aharonian, F. A., Crocker, R. M., & Jones, D. I. 2011, *ApJ*, 726, 60
- Dunkel, J., Talkner, P., & Hänggi, P. 2007, *Phys. Rev. D*, 75, 043001
- Fujita, Y., Murase, K., & Kimura, S. S. 2016, ArXiv e-prints, arXiv:1604.00003
- Gabici, S. 2011, *Mem. Soc. Astron. Italiana*, 82, 760
- Genzel, R., Eisenhauer, F., & Gillessen, S. 2010, *Reviews of Modern Physics*, 82, 3121
- Guo, Y.-Q., Tian, Z., Wang, Z., Li, H.-J., & Chen, T.-L. 2016, ArXiv e-prints, arXiv:1604.08301
- HESS Collaboration, Abramowski, A., Aharonian, F., et al. 2016, *Nature*, 531, 476
- Hills, J. G. 1975, *Nature*, 254, 295
- Hinton, J. A., & Aharonian, F. A. 2007, *ApJ*, 657, 302
- Kelner, S. R., Aharonian, F. A., & Bugayov, V. V. 2006, *Phys. Rev. D*, 74, 034018
- Komossa, S. 2015, *Journal of High Energy Astrophysics*, 7, 148
- Liu, S., Melia, F., Petrosian, V., & Fatuzzo, M. 2006, *ApJ*, 647, 1099
- Livio, M., & Waxman, E. 2000, *ApJ*, 538, 187
- Malkov, M. A., Diamond, P. H., Sagdeev, R. Z., Aharonian, F. A., & Moskalenko, I. V. 2013, *ApJ*, 768, 73
- Moskalenko, I. V., Porter, T. A., & Strong, A. W. 2006, *ApJ*, 640, L155
- Paglione, T. A. D., & Abrahams, R. D. 2012, *ApJ*, 755, 106
- Peng, F.-K., Wang, X.-Y., Liu, R.-Y., Tang, Q.-W., & Wang, J.-F. 2016, *ApJ*, 821, L20
- Porter, T. A., & Strong, A. W. 2005, *International Cosmic Ray Conference*, 4, 77
- Prosekin, A. Y., Kelner, S. R., & Aharonian, F. A. 2015, *Phys. Rev. D*, 92, 083003
- Ptuskin, V. S., & Khazan, Y. M. 1981, *Soviet Ast.*, 25, 547
- Rees, M. J. 1988, *Nature*, 333, 523



- Said, S. S., Wolfendale, A. W., Giler, M., & Wdowczyk, J. 1981, International Cosmic Ray Conference, 2, 344
- Stone, N. C., & Metzger, B. D. 2016, MNRAS, 455, 859
- Strong, A. W., Porter, T. A., Digel, S. W., et al. 2010, ApJ, 722, L58
- Uchiyama, Y., Funk, S., Katagiri, H., et al. 2012, ApJ, 749, L35
- Wang, J., & Merritt, D. 2004, ApJ, 600, 149
- Zhang, J.-L., Bi, X.-J., & Hu, H.-B. 2006, A&A, 449, 641